

Rabi oscillation and electron-spin-echo envelope modulation of the photoexcited triplet spin system in silicon

Waseem Akhtar,¹ Takeharu Sekiguchi,¹ Tatsumasa Itahashi,¹ Vasileia Filidou,² John J. L. Morton,^{2,3} Leonid Vlasenko,⁴ and Kohei M. Itoh^{1,*}

¹*School of Fundamental Science and Technology, Keio University, 3-14-1 Hiyoshi, Kohoku-ku, Yokohama 223-8522, Japan*

²*Department of Materials, University of Oxford, Parks Road, Oxford OXI 3PH, United Kingdom*

³*London Centre for Nanotechnology, University College London, 17-19 Gordon Street, London WC1H 0AH, United Kingdom*

⁴*A. F. Ioffe Physico-Technical Institute, Russian Academy of Sciences, 194021 St. Petersburg, Russia*

(Received 11 March 2012; revised manuscript received 30 July 2012; published 11 September 2012)

We report on a pulsed electron paramagnetic resonance (EPR) study of the photoexcited triplet state ($S = 1$) of oxygen-vacancy centers in silicon. Rabi oscillations between the triplet sublevels are observed using coherent manipulation with a resonant microwave pulse. The Hahn echo and stimulated echo decay profiles are superimposed with strong modulations known as electron-spin-echo envelope modulation (ESEEM). The ESEEM spectra reveal a weak but anisotropic hyperfine coupling between the triplet electron spin and a ^{29}Si nuclear spin ($I = 1/2$) residing at a nearby lattice site, that cannot be resolved in conventional field-swept EPR spectra.

DOI: [10.1103/PhysRevB.86.115206](https://doi.org/10.1103/PhysRevB.86.115206)

PACS number(s): 76.30.-v, 71.55.Cn, 76.60.Lz, 03.67.Lx

I. INTRODUCTION

Nuclear spins in solid-state systems are potential candidates for quantum bits owing to their long coherence times.¹⁻⁴ Among them, the ^{29}Si nuclear spin has been attracting attention since the proposal of an all-silicon quantum computer architecture utilizing the ^{29}Si nuclear spins embedded in a spin-free ^{28}Si matrix,^{5,6} which was followed by experimental demonstration of an extremely long ^{29}Si nuclear spin coherence time in silicon using rf decoupling techniques.² Despite such attractive properties, ^{29}Si nuclear spin qubits suffer from weak thermal polarization under experimentally accessible conditions and thus are difficult to be initialized. Furthermore, the intrinsic dipolar interactions between nuclear spins are very weak, limiting the speed of quantum logic gate operations. Such limitations for nuclear spin qubits can be overcome by utilizing their hyperfine coupling with an electron spin. A coherent state of the electron spin can be transferred to a hyperfine-coupled nuclear spin using the SWAP operation.^{1,7} However, the nuclear spin coherence time is then limited by the spin-relaxation time of the coupled electron spin.

Hyperfine coupling to a photoexcited electron spin-triplet has advantages as follows. The high (nonequilibrium) electron spin polarization of the photoexcited triplet can be used to initialize the coupled nuclear spins⁸ and to mediate entanglement between the nuclear spin qubits on time scales much faster than their intrinsic dipolar coupling, thus leading to faster quantum logic operations.^{9,10} Moreover, as the ground state of the electron spin is a singlet, it will not have an impact on nuclear spin dephasing. The optical excitation to the electron spin triplet and deexcitation via spin-orbit coupling to the ground singlet state would further allow to switch on and off certain interactions between the nuclear spins. Taking advantage of these properties, we have demonstrated recently that the strong hyperfine coupling of the photoexcited triplet oxygen-vacancy center (SL1 center) in silicon can be used to address, initialize, and coherently manipulate nearby ^{29}Si

nuclear spins.¹¹ Such a photoexcited triplet could further be used to entangle two remote ^{29}Si nuclear spins in the lattice. To date, however, only the two nearest-neighbor ^{29}Si nuclear spins have been resolved in electron paramagnetic resonance (EPR) spectroscopy of the SL1 center.^{12,13} In this work we utilize the high resolution of the electron-spin-echo envelope modulation (ESEEM) technique^{14,15} to reveal the hyperfine interaction of the triplet with the nuclear spin of ^{29}Si at different lattice sites that cannot be resolved in conventional EPR spectroscopy.

The oxygen-vacancy (O-V) defect created by high-energy electron-beam irradiation of Czochralski (CZ)-grown silicon can be excited into the triplet SL1 center with above-band-gap illumination.^{12,16,17} The spin Hamiltonian for an $S = 1$ spin system under magnetic field \mathbf{B}_0 can be described as $\mathcal{H}_e = \mu_B \mathbf{B}_0 \cdot \mathbf{g}_e \cdot \mathbf{S} + hD(S_Z^2 - S^2/3) + hE(S_X^2 - S_Y^2)$, where \mathbf{g}_e is the electron-spin g -tensor; μ_B is the Bohr magneton; D and E are the zero-field parameters; and X , Y , and Z are the principal axes of the defect. For the SL1 center, \mathbf{g}_e is nearly isotropic, and $D = -985.4$ MHz and $E = 21.5$ MHz.^{12,18} These EPR parameters, the defect structure, and the nonequilibrium polarization in this spin system have been revealed by various EPR studies.^{11-13,19-21} Here we focus on two of the various possible crystallographic orientations of the SL1 center in silicon as illustrated in Fig. 1(a). When the magnetic field \mathbf{B}_0 is rotated in the (110) plane, the angle of \mathbf{B}_0 with respect to the direction \mathbf{r} joining the two vacancy-bridged silicon atoms (i and j lattice sites) varies from 0° to 360° for the SL1⁰ orientation, while this angle is constant at 90° for the SL1⁹⁰ orientation. The first-derivative cw-EPR spectrum of the SL1 center with $\mathbf{B}_0 \parallel [1\bar{1}0]$ is shown in Fig. 1(b). The four main peaks originate from different defect orientations (SL1⁰ and SL1⁹⁰) and different EPR transitions¹² as labeled. The two satellite peaks for every main peak are attributed¹² to the strong hyperfine interaction of the triplet spin ($S = 1$) with the ^{29}Si nuclear spin ($I = 1/2$) situated at either site i or site j in Fig. 1(a).

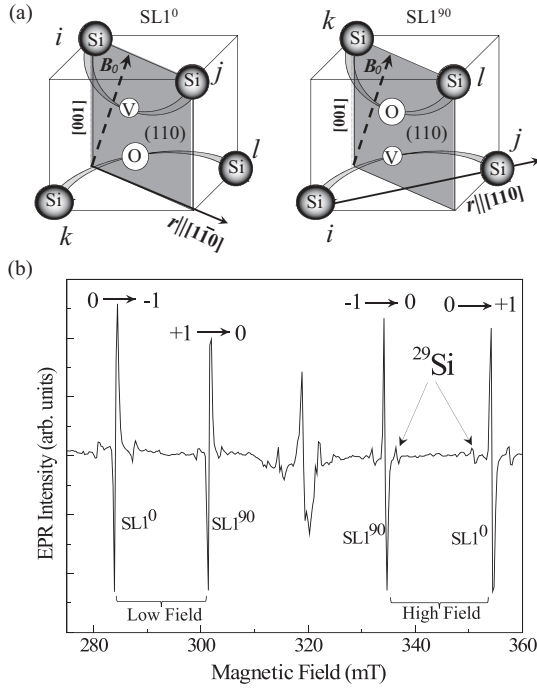


FIG. 1. (a) $SL1^0$ and $SL1^{90}$ orientations of the photoexcited triplet center (O-V defect) in silicon crystal. The vector r represents the direction joining the silicon atoms at i and j lattice sites bridged by the vacancy. (b) EPR spectrum of the SL1 center at $T = 12$ K for the applied magnetic field of $B_0 \parallel [1\bar{1}0]$. The main peaks for the $SL1^0$ and $SL1^{90}$ orientations are marked with the electron spin projections on the B_0 axis, m_S , of the initial and final states involved in the corresponding EPR transition. The satellite peaks are due to the strong hyperfine interaction with the ^{29}Si ($I = 1/2$) sitting at either lattice site i or lattice site j .¹²

II. EXPERIMENT

The experiments were performed with a rectangular sample cut from a CZ-grown, natural abundant silicon (4.7% ^{29}Si) wafer that had been exposed to room-temperature irradiation of a 1-MeV electron beam with a dose of 10^{18} cm^{-2} . Pulsed EPR experiments were performed using a JEOL pulse EPR spectrometer working at X-band. The sample was mounted in an Oxford helium flow cryostat to achieve low temperatures in the range 5–20 K. A 1047-nm Nd:YLF laser with an output power of 280 mW was used for continuous optical excitation. The pulse sequences used for the Hahn echo and stimulated echo measurements are described in the next section.

III. RESULTS AND DISCUSSION

A. Rabi oscillation and echo decay

Continuous optical excitation populates all the triplet sublevels equally, but different nonradiative decay rates from the triplet sublevels to the ground singlet state build up a spin polarization.¹¹ Under the continuous optical excitation, resonant microwave pulses are applied at each main peak in Fig. 1(b) to coherently manipulate the triplet spins between two magnetic sublevels involved in the EPR transition. Rabi

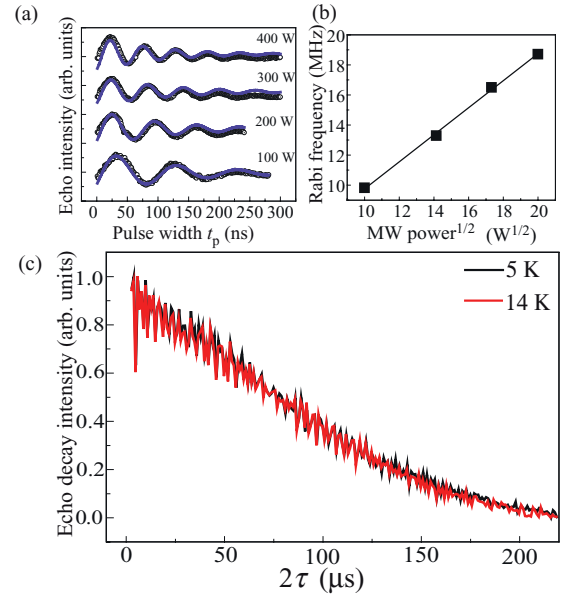


FIG. 2. (Color online) (a) Rabi oscillation observed as a function of microwave pulse width t_p for the $m_S = -1$ to $m_S = 0$ transition of the $SL1^{90}$ center with $B_0 = 334.5$ mT parallel to the $[1\bar{1}0]$ direction. Circles (o) are the experimental data for different powers of resonant microwave, and each blue line represents the fitting to a damped sine function. (b) The microwave power dependence of the Rabi frequency. (c) Echo decay profiles measured by the Hahn echo pulse sequence ($\pi/2$ - τ - π - τ -echo) at two different temperatures.

oscillations are observed by measuring the echo intensity as a function of the first-pulse duration t_p , for which the microwave pulse sequence is t_p - τ - π - τ -echo. Figure 2(a) shows Rabi oscillations of the triplet electron spin between the $m_S = 0$ and $m_S = -1$ states of the $SL1^{90}$ center for different microwave powers. The observed Rabi oscillations (circles) at each power are fitted to a damped sine function (blue curve). As expected, the observed Rabi frequency scales linearly with the magnitude of the applied microwave field [Fig. 2(b)]. The fast damping of the oscillation is primarily due to the inhomogeneity of the static and the resonant microwave field in the EPR cavity.^{22–24}

Figure 2(c) shows the spin-echo decay profiles under continuous photoexcitation measured with the Hahn echo pulse sequence ($\pi/2$ - τ - π - τ -echo) at two different temperatures. No dependence on the temperature is observed in the range 5–20 K, indicating that the coherence is not limited by the temperature-sensitive spin-lattice (T_1) relaxation mechanism.²⁵ We also find that the echo decay is independent of the defect orientation.^{25–27} These results suggest that the dominant decoherence mechanisms of this triplet electron spin are the interaction with other optically excited electron spins as well as the decay of the triplet into the ground singlet state. To substantiate this, we employ pulsed-laser excitation for the Hahn echo measurement, in which the microwave pulses are applied after the pulsed optical excitation. (Further details of the experimental setup are described in Ref. 11.) Figure 3 shows that the echo decay is much slower with pulsed optical excitation than with continuous excitation. The single exponential fit to the echo decay curve obtained under pulsed

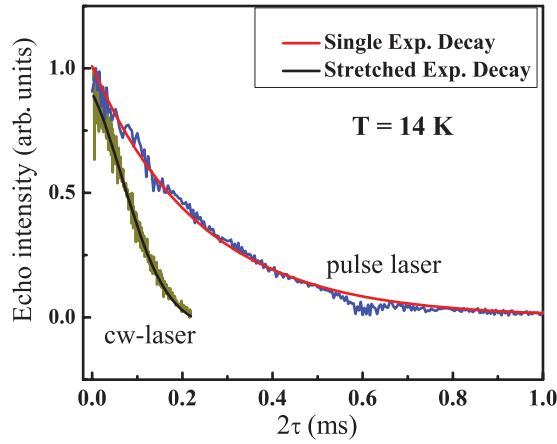


FIG. 3. (Color online) An echo decay profile under pulsed-laser excitation (blue points) is fitted to a single exponential function $\exp[-2\tau/T_m]$ (red curve), where T_m is the decoherence time. An echo decay profile under cw-laser excitation (light green) is fitted to a stretched exponential $\exp[-2\tau/T_m - (2\tau/T_{SD})^2]$ since the single exponential does not yield a good fit.²⁸ Here, T_{SD} represents the time constant related to the effect of optical excitation on the decoherence of the electron spin. Fitted curves shown for $T_m = 240 \mu\text{s}$ and $T_{SD} = 153 \mu\text{s}$.

excitation gives a time constant of $240 \pm 4 \mu\text{s}$, which is close to the lifetime of the faster decaying triplet sublevel involved in the EPR transition.¹¹ Thus, decoherence of the SL1 triplet electron spin under continuous or pulsed optical excitation is caused predominantly by effects of the optical excitation itself and the subsequent decay of the triplet.

B. Electron-spin-echo envelope modulation (ESEEM)

The echo decay profiles in Fig. 2(c) show a strong modulation known as ESEEM. This is caused by the anisotropic hyperfine interaction of the electron spin with neighboring nuclear spins.¹⁴ For ESEEM analysis, the Hamiltonian of a single $S = 1$ electron spin interacting with a nuclear spin of I can be represented by

$$\mathcal{H}_{e-n} = \mathcal{H}_e - \mu_n g_n B_0 I_z + h A S_z I_z + h B S_z I_x.$$

Here g_n is the g -factor of the nuclear spin and μ_n is the nuclear magneton, while A and B represent the secular and pseudosecular terms of the hyperfine coupling in units of frequency and depend on the field orientation z with respect to the defect axes. The pseudosecular term makes the hyperfine-coupled nuclear spin quantized along an effective magnetic field direction tilted from the electron-spin quantization axis z . This tilt leads to mixing of the nuclear spin states, so that application of an intense microwave pulse excites not only the EPR-allowed transitions but also the EPR-forbidden transitions that involve nuclear spin flipping. The interference between these transitions generates beats in the electron-spin-echo decay curve. Figure 4(a) shows the splitting of the triplet sublevels due to the hyperfine interaction with an $I = 1/2$ nuclear spin. The nuclear magnetic resonance (NMR)

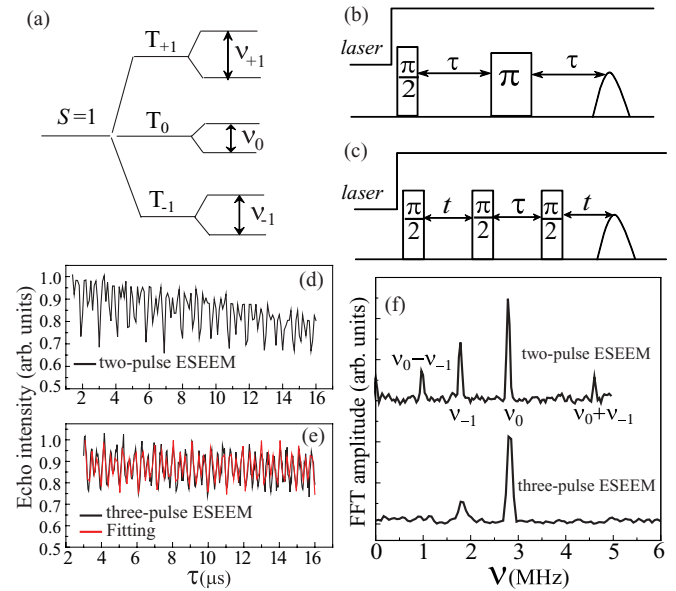


FIG. 4. (Color online) (a) Energy levels of the SL1 triplet electron spin interacting with a nuclear spin $I = 1/2$. The pulse sequences employed for observing (b) two-pulse and (c) three-pulse ESEEM. (d) Two-pulse ESEEM and (e) three-pulse ESEEM traces, for the $m_S = -1$ to $m_S = 0$ transition of the SL1⁹⁰ orientation at $B_0 = 334.5 \text{ mT}$ parallel to the $[1\bar{1}0]$. The $\pi/2$ pulse had a duration of 20 ns, and t is fixed at 800 ns. The red curve is the fit of the experimental data to the theoretical expression for the three-pulse ESEEM.¹⁵ (f) The frequency-domain spectra obtained by Fourier transformation of the ESEEM signals [(d) and (e)] after subtracting the exponential decay component.

frequency of the m_S sublevel is given to the first order by¹⁵

$$v_{m_S} = \sqrt{(m_S A - v_I)^2 + (m_S B)^2}, \quad (1)$$

where $v_I = g_n \mu_n B_0 / h$ represents the signed, Zeeman frequency of the nuclear species causing modulations. Note here that v_I is negative for negative g_n , but $v_0 = |v_I|$ is always positive. The *intrinsic* modulation amplitude is given by the modulation depth parameter¹⁵ $K_{\alpha,\beta} = (v_I B / v_\alpha v_\beta)^2$, where v_α and v_β represent the NMR frequencies in the two electron-spin sublevels involved in the EPR transition. In particular, for $S = 1$, the modulation depth expression reduces to

$$K_{\pm 1} = (B / v_{\pm 1})^2, \quad (2)$$

since either v_α or v_β always coincides with $v_0 = |v_I|$. Substitution of Eq. (1) into Eq. (2) shows a constraint on K : $0 \leq K \leq 1$. For the two-pulse ESEEM obtained by the Hahn echo sequence [Fig. 4(b)], the modulation involves the two fundamental frequencies (v_α, v_β) and also the sum and difference of these frequencies.

Figure 4(d) shows the two-pulse ESEEM trace from the SL1⁹⁰ center for the $m_S = -1$ to $m_S = 0$ transition ($B_0 = 334.5 \text{ mT}$). The frequency-domain spectrum obtained by Fourier transform of this two-pulse ESEEM signal after removal of the decay part by a single exponential fitting is shown in Fig. 4(f). The peak frequencies of 2.8 and 1.8 MHz can be assigned to the fundamental frequencies v_0 and v_{-1} involved in

the modulation, while 4.6 and 1.0 MHz are the sum and difference of these frequencies. In order to confirm this assignment, we also perform three-pulse ESEEM (based on a stimulated echo) with the sequence $\pi/2-t-\pi/2-\tau-\pi/2-t$ -echo. The second $\pi/2$ pulse transfers the electron-spin coherence into a nuclear spin coherence. During the evolution time τ this decays with the nuclear spin coherence time T_{2n} , which should be on the order of the electron-spin-lattice relaxation time T_{1e} . Hence an echo can be observed out to much longer time delays as compared to two-pulse ESEEM. The third $\pi/2$ pulse transfers the nuclear spin coherence back to the observable electron-spin coherence. The added advantage of the three-pulse ESEEM experiment lies in the fact that the modulation as a function of the second interval τ contains only the fundamental frequencies, resulting in a much simpler spectrum. The three-pulse ESEEM signal and its Fourier-transformed spectrum for the same EPR transition as used for the two-pulse ESEEM [Fig. 4(d)] are shown in Figs. 4(e) and 4(f), respectively. As expected, only two peaks are seen at 2.8 and 1.8 MHz. This result allows us to conclude that they are the NMR frequencies ν_0 and ν_{-1} of the triplet sublevels involved in the EPR transition. The natural silicon sample contains 4.7% ^{29}Si , the only stable isotope of silicon with a nonzero nuclear spin ($I = 1/2$), and its nuclear g -factor¹² $g_n = -1.111$ corresponds to the nuclear Zeeman frequency of $\nu_I = -2.8$ MHz at 334.5 mT used for the ESEEM measurements [Fig. 4]. Therefore, we conclude that the observed modulation is due to the hyperfine interaction with a ^{29}Si nuclear spin and that the frequencies of 2.8 and 1.8 MHz correspond to the NMR frequencies of the $m_S = 0$ and $m_S = -1$ sublevels, respectively, of the SL1^{90} center (334.5 mT). Thus, the ESEEM experiments reveal weak hyperfine coupling (<5 MHz) between the SL1 triplet electron spin and a ^{29}Si nuclear spin that cannot be resolved in the field-swept EPR spectrum.²⁹

ESEEM is also observed for the SL1^0 orientation at the resonance between $m_S = 0$ and $m_S = +1$ ($B_0 = 353.9$ mT), in which the modulation frequencies are found to be $\nu_0 = 3.0$ MHz, $\nu_{+1} = 0.6$ MHz, as well as their sum (3.6 MHz) and difference (2.4 MHz). According to Eq. (1), the experimental results of $\nu_{+1} < \nu_0$ for the SL1^0 orientation and $\nu_{-1} < \nu_0$ for the SL1^{90} orientation reveal that the sign of the secular hyperfine term A depends on the defect orientation, i.e., $A < 0$ for the SL1^0 and $A > 0$ for the SL1^{90} . In more details, the observed modulation frequencies give the estimation for the value of A : $-3.6 < A < -2.4$ MHz for the SL1^0 and $+1.0 < A < +4.6$ MHz for the SL1^{90} . Such an anisotropic nature of the hyperfine interaction indicates that the remote dipolar hyperfine coupling is at least as strong as the Fermi-contact hyperfine coupling, allowing the pseudosecular term B as strong as the secular term A . This is required for strong modulation in the ESEEM trace according to Eqs. (1) and (2) and confirmed in our experiments.

In contrast, at the low-field lines for both the SL1^0 and SL1^{90} orientations, we observe modulation only with the nuclear Zeeman frequency ($\nu_0 = |\nu_I| \propto B_0$) in the ESEEM traces. The absence of the ν_{-1} (ν_{+1}) modulation at the low-field line of the SL1^0 (SL1^{90}) center is consistent with the theoretical estimation of the modulation amplitudes at the low-field lines using Eqs. (1), (2), and the observed modulation frequencies

at the corresponding high-field lines. In fact, the ratio of the modulation depth at the low-field line (LF) to the depth at the high-field line (HF), $R = K^{\text{LF}}/K^{\text{HF}}$, can be estimated to be $6.3\% < R < 25\%$ and $1.0\% < R < 1.6\%$ for the SL1^{90} and SL1^0 , respectively, predicting a much weaker modulation at the low-field lines. For the same reason and due to the complicated rotation pattern¹² of the EPR spectra, we could not obtain detailed angular dependence of the ESEEM spectra. However, a small tilt of the magnetic field from a high-symmetry direction gives useful information for the ^{29}Si site assignment as discussed below.

C. Site assignment of ^{29}Si nuclear spin contributing to ESEEM

The ESEEM technique has been used also for other paramagnetic centers in silicon. The ESEEM spectra of phosphorus donors in ^{29}Si -enriched silicon showed a predominant contribution from the hyperfine coupling with ^{29}Si at the four equivalent nearest-neighbor sites,³⁰ while hyperfine coupling with ^{29}Si for at least five different sites was required to reproduce the ESEEM trace of the P_b center at the oxide interface of ^{29}Si -enriched silicon.³¹ For the SL1 center, the ^{29}Si at two sites, i and j , of the four nearest neighbors as illustrated in Fig. 1(a) has strong enough hyperfine coupling to be resolved as satellite peaks in the EPR spectrum¹² as in Fig. 1(b), so they cannot contribute to the observed ESEEM. Considering the localized nature of the SL1 triplet state,¹² let us assume that the ^{29}Si at the other two nearest-neighbor sites k and i [Fig. 1(a)] give a dominant contribution to the ESEEM. This assignment is consistent with the splitting observed in the ESEEM spectrum when the magnetic field is tilted from the $[1\bar{1}0]$ axis. Figure 5 shows the two-pulse ESEEM spectrum obtained from the $m_S = -1$ to $m_S = 0$ transition of the SL1^{90} center with the magnetic field ($B_0 = 333.8$ mT) tilted by 15° from the $[1\bar{1}0]$ direction within the (110) plane. Under this condition, the positions of the k and i sites, viewed from the

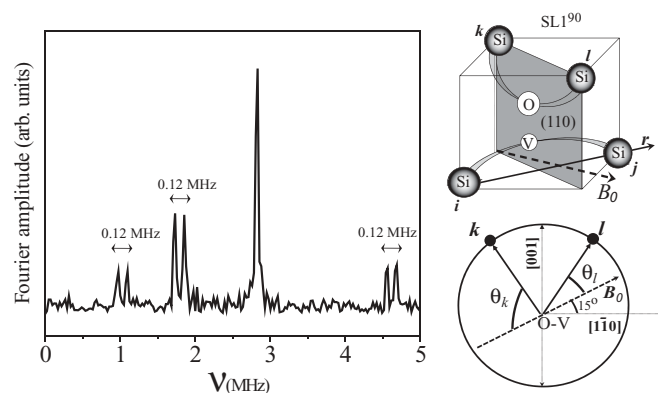


FIG. 5. A Fourier-transformed spectrum of the two-pulse ESEEM for the SL1^{90} center with the magnetic field B_0 (337.8 mT) rotated around the $[110]$ axis by an angle of 15° from the $[1\bar{1}0]$ direction. Splitting of 0.12 MHz is seen for each line at 1.0, 1.8, and 4.6 MHz, and it can be attributed to the nonequivalent ^{29}Si sites, k and i , as the magnetic field is rotated in the (110) plane. The line ν_0 at 2.8 MHz is unsplit because of no first-order hyperfine interaction for the $m_S = 0$ sublevel.

triplet electron spin which should be localized predominantly around the vacancy site, make different angles with respect to the applied field direction, and hence these two ^{29}Si sites should have different values for both secular and pseudosecular hyperfine terms (A, B). The observed splitting (0.12 MHz) for all but the 2.8-MHz peak can be explained by this kind of anisotropy in the hyperfine coupling, associated with the symmetry of the assumed nuclear spin sites. The absence of splitting at 2.8 MHz is expected because the nuclear spin has no first-order hyperfine coupling with the electron spin in the $m_S = 0$ state; i.e., the ESEEM frequency ν_0 is determined only by the nuclear Zeeman interaction, which is independent of the field orientation. It should be noted that we cannot completely exclude other assignments of the ESEEM-contributing nuclear spin sites. For the magnetic field within the (110) plane, another pair of sites may have the same site symmetry as the k and l sites, i.e., the reflection symmetry about the $(1\bar{1}0)$ plane containing the O-V axis. Such pair sites are present, e.g., among the 12 next-nearest-neighbor sites: the pair of equivalent sites bonded to the k or l site and located in the $[1\bar{1}0]$ direction with respect to the O-V core, the other two pairs bonded to the k or l site but not in the $[1\bar{1}0]$ direction, and two similar pairs bonded to the i or j site.

The pseudosecular hyperfine parameter $|B|$ could be determined if the *intrinsic* modulation depth K is known, as it is directly related to the hyperfine parameters as in Eq. (2). However, the ^{29}Si concentration f_{29} in our sample is only 4.7%. Hence, the *apparent* modulation amplitude \tilde{K} as observed in the ESEEM spectra should be much smaller than the *intrinsic* modulation depth. Estimation of $|B|$ requires the probability P_{29} that the ESEEM-contributing lattice sites are occupied by the ^{29}Si isotope, which depends on f_{29} and the number of equivalent sites N_s contributing to the ESEEM: $P_{29}(N_s, f_{29}) = N_s C_1 f_{29} (1 - f_{29})^{N_s - 1}$ for the single occupation of the equivalent sites and $\tilde{K} = P_{29} K$. A further complication arises in that the effect of ^{29}Si nuclear spins with much weaker hyperfine coupling also appears in the ESEEM spectra as evidenced by the fact that the peak amplitude at the nuclear Zeeman frequency (ν_0) is significantly stronger than the $\nu_{\pm 1}$ amplitude. Note that the half amplitude of the sum and difference frequency peaks compared to the $\nu_{\pm 1}$ peak is just as expected from the theory.¹⁵ The greater intensity of the ν_0 peak can be explained by non-negligible contribution to the ν_0 modulation from distant ^{29}Si sites, since ν_0 is independent of the hyperfine coupling strength (A, B) and the number of such sites can be very large even though they have much weaker hyperfine coupling. Considering these effects and based on the theoretical function given in Ref. 15, the fitting of the three-pulse ESEEM trace [Fig. 4(e)] of the SL1^{90} center measured at its high-field line yields $\tilde{K}_{-1} \approx 9\%$ for the *apparent* modulation amplitude of the ν_{-1} component. By the

same means, $\tilde{K}_{+1} \approx 10\%$ is obtained for the SL1^0 center at its high-field line. If the ESEEM-contributing lattice sites have twofold degeneracy ($N_s = 2$) such as the nearest-neighbor k and l sites, the ^{29}Si occupation probability is $P_{29}(2, 4.67\%) = 8.9\%$ for our sample. Considering the fitting uncertainties for the determination of the *apparent* modulation amplitude \tilde{K} , the *intrinsic* modulation depth parameter K is estimated to be roughly 100% for both the SL1^0 and SL1^{90} orientations. Therefore, N_s cannot be less than 2 to satisfy $K \leq 100\%$, giving the upper limit of the pseudosecular hyperfine term $|B|$ by $\nu_{\pm 1}$, i.e., 0.6 and 1.8 MHz for SL1^0 and SL1^{90} , respectively. This limitation on N_s is consistent with the splitting as observed in Fig. 5, and still we cannot exclude the possibility of $N_s = 4$ (or higher degeneracy) such as the next-nearest-neighbor sites mentioned above. Even if B is determined, A cannot be uniquely determined from a single ESEEM spectrum. Determination of the hyperfine parameters (A, B) and the ^{29}Si sites contributing to the ESEEM spectra requires further investigation, e.g., a more detailed angular dependence study of the ESEEM spectra, using Si:SL1 samples containing different concentrations of ^{29}Si isotope, using either electron-nuclear double resonance (ENDOR) spectroscopy or ESEEM spectroscopy at higher fields to increase the resolution, and calculating the SL1 triplet state wave function to simulate the hyperfine parameters from first principles.

IV. CONCLUSION

In summary, we have reported the experimental demonstration of the coherent manipulation of electron spins of the photoexcited triplet center SL1 in silicon. The electron spin is coherently manipulated by the microwave pulse as indicated by the Rabi oscillations. The electron-spin coherence time is short under continuous photoexcitation but can be extended by use of pulsed photoexcitation to a duration limited by the triplet decay lifetime (≈ 0.3 ms). Strong modulations of the electron-spin-echo decay curves reveal the anisotropic hyperfine coupling of the triplet electron spin with a ^{29}Si nuclear spin at one of a number of neighboring sites that have not been resolved in a conventional EPR spectrum.

ACKNOWLEDGMENTS

We thank Fujitsu Laboratories Ltd. for providing us with the opportunities to use their pulse EPR system. The work at Keio was supported in part by Grant-in-Aid for Scientific Research No. 22241024 and the Project for Developing Innovation Systems by MEXT, in part by FIRST, and in part by JST-EPSRC/SIC (Grant No. EP/H025952/1). The work at Oxford was supported by the EPSRC through CAESR (Grant No. EP/D048559/1).

*kitoh@appi.keio.ac.jp

¹J. J. L. Morton, A. M. Tyryshkin, R. M. Brown, S. Shankar, B. W. Lovett, A. Ardavan, T. Schenkel, E. E. Haller, J. W. Ager, and S. A. Lyon, *Nature (London)* **455**, 1085 (2008).

²T. D. Ladd, D. Maryenko, Y. Yamamoto, E. Abe, and K. M. Itoh, *Phys. Rev. B* **71**, 014401 (2005).

³M. Steger, K. Saeedi, M. L. W. Thewalt, J. J. L. Morton, H. Riemann, N. V. Abrosimov, P. Becker, and H.-J. Pohl, *Science* **336**, 1280 (2012).

⁴P. C. Maurer, G. Kucsko, C. Latta, L. Jiang, N. Y. Yao, S. D. Bennett, F. Pastawski, D. Hunger, N. Chisholm, M. Markham, D. J. Twitchen, J. I. Cirac, and M. D. Lukin, *Science* **336**, 1283 (2012).

- ⁵T. D. Ladd, J. R. Goldman, F. Yamaguchi, Y. Yamamoto, E. Abe, and K. M. Itoh, *Phys. Rev. Lett.* **89**, 017901 (2002).
- ⁶K. M. Itoh, *Solid State Commun.* **133**, 747 (2005).
- ⁷R. M. Brown, A. M. Tyryshkin, K. Porfyrakis, E. M. Gauger, B. W. Lovett, A. Ardavan, S. A. Lyon, G. A. D. Briggs, and J. J. L. Morton, *Phys. Rev. Lett.* **106**, 110504 (2011).
- ⁸J. Schmidt, D. J. van den Heuvel, A. Henstra, T.-S. Lin, and W. Wenckebach, *Pure Appl. Chem.* **64**, 859 (1992).
- ⁹M. Schaffry, V. Filidou, S. D. Karlen, E. M. Gauger, S. C. Benjamin, H. L. Anderson, A. Ardavan, G. A. D. Briggs, K. Maeda, K. B. Henbest, F. Giustino, J. J. L. Morton, and B. W. Lovett, *Phys. Rev. Lett.* **104**, 200501 (2010).
- ¹⁰V. Filidou, S. Simmons, S. D. Karlen, H. L. Anderson, F. Giustino, and J. J. L. Morton, *Nat. Phys.* **8**, 596 (2012).
- ¹¹W. Akhtar, V. Filidou, T. Sekiguchi, E. Kawakami, T. Itahashi, L. Vlasenko, J. J. L. Morton, and K. M. Itoh, *Phys. Rev. Lett.* **108**, 097601 (2012).
- ¹²K. L. Brower, *Phys. Rev. B* **4**, 1968 (1971).
- ¹³L. S. Vlasenko, I. M. Zaritskii, A. A. Konchits, and B. D. Shanina, *Sov. Phys. Solid State* **26**, 66 (1984).
- ¹⁴W. B. Mims, *Phys. Rev. B* **5**, 2409 (1972).
- ¹⁵A. Schweiger and G. Jeschke, *Principles of Pulse Electron Paramagnetic Resonance* (Oxford University Press, New York, 2001).
- ¹⁶G. D. Watkins, J. W. Corbett, and R. M. Walker, *J. Appl. Phys.* **30**, 1198 (1959).
- ¹⁷J. W. Corbett, G. D. Watkins, R. M. Chrenko, and R. S. McDonald, *Phys. Rev.* **121**, 1015 (1961).
- ¹⁸L. S. Vlasenko, M. P. Vlasenko, V. N. Lomasov, and V. A. Khramtsov, *Sov. Phys. JETP* **64**, 612 (1986).
- ¹⁹B. Stich, S. Greulich-Weber, and J. M. Spaeth, *J. Appl. Phys.* **77**, 1546 (1995).
- ²⁰W. Akhtar, H. Morishita, L. S. Vlasenko, D. S. Poloskin, and K. M. Itoh, *Physica B* **404**, 4583 (2009).
- ²¹W. Akhtar, H. Morishita, K. Sawano, Y. Shiraki, L. S. Vlasenko, and K. M. Itoh, *Phys. Rev. B* **84**, 045204 (2011).
- ²²H. C. Torrey, *Phys. Rev.* **56**, 1059 (1949).
- ²³J. J. L. Morton, A. M. Tyryshkin, A. Ardavan, K. Porfyrakis, S. A. Lyon, and G. A. D. Briggs, *Phys. Rev. A* **71**, 012332 (2005).
- ²⁴L. M. K. Vandersypen and I. L. Chuang, *Rev. Mod. Phys.* **76**, 1037 (2004).
- ²⁵A. M. Tyryshkin, S. A. Lyon, A. V. Astashkin, and A. M. Raitsimring, *Phys. Rev. B* **68**, 193207 (2003).
- ²⁶R. de Sousa and S. Das Sarma, *Phys. Rev. B* **68**, 115322 (2003).
- ²⁷Decoherence induced by flip-flops of surrounding ²⁹Si nuclear spins depends on orientation.^{25,26} Therefore we neglect its effect on decoherence of the triplet SL1 electron spin.
- ²⁸At present we do not have solid reason for the power of 2 in the stretched exponential fitting for the cw photoexcitation, but we assume that the optical excitation causes random fluctuation of the electron-spin environment leading to a spectral diffusion similar to that observed on the echo decay of the phosphorus donor electron spins in silicon caused by the flip-flops of ²⁹Si nuclear spins.³⁰
- ²⁹In Ref. 12, the shoulders at the main peaks observed in EPR spectra were attributed to hyperfine splitting of ≈ 18 MHz on average due to six unidentified ²⁹Si sites. However, such a large hyperfine splitting is not observed in our ESEEM spectra probably due to its limited spectral bandwidth given by the pulse width and the τ increment.
- ³⁰E. Abe, A. M. Tyryshkin, S. Tojo, J. J. L. Morton, W. M. Witzel, A. Fujimoto, J. W. Ager, E. E. Haller, J. Isoya, S. A. Lyon, M. L. W. Thewalt, and K. M. Itoh, *Phys. Rev. B* **82**, 121201(R) (2010).
- ³¹F. Hoehne, J. Lu, A. R. Stegner, M. Stutzmann, M. S. Brandt, M. Rohrmüller, W. G. Schmidt, and U. Gerstmann, *Phys. Rev. Lett.* **106**, 196101 (2011).